Electronic structure and stability of quaternary chalcogenide semiconductors derived from cation cross-substitution of II-VI and I-III-VI$_2$ compounds

Shiyou Chen and X. G. Gong

Department of Physics, MOE Key Laboratory of Computational Physical Sciences and Surface Science Laboratory, Fudan University, Shanghai 200433, China

Aron Walsh and Su-Huai Wei

National Renewable Energy Laboratory, Golden, Colorado 80401, USA

Sequential cation cross-substitution in zinc-blende chalcogenide semiconductors, from binary to ternary to quaternary compounds, is systematically studied using first-principles electronic structure calculations. Several universal trends are found for the ternary and two classes of quaternary chalcogenides, for example, the lowest-energy structure always has larger lattice constant a, smaller tetragonal distortion parameter $\eta = c/2a$, negative crystal-field splitting at the top of the valence band, and larger band gap compared to the metastable structures for common-row cation substitution. The band structure changes in the cation substitution are analyzed in terms of the band offsets and band character decomposition, showing that although the band gap decreases from binary II-VI to ternary I-III-VI$_2$ are mostly due to the $p-d$ repulsion in the valence band, the decreases from ternary I-III-VI$_2$ to quaternary I$_2$-II-IV-VI$_4$ chalcogenides are due to the downshift in the conduction band caused by the wave-function localization on the group IV cation site. We propose that common-row-cation I$_2$-II-IV-VI$_4$ compounds are more stable in the kesterite structure, whereas the widely assumed stannite structure reported in the literature for experimental samples is most likely due to partial disorder in the I-II (001) layer of the kesterite phase.

PACS number(s): 61.50.Ah, 71.20.Nr, 71.22.+i, 71.70.Fk

I. INTRODUCTION

The design and synthesis of adamantine multiternary chalcogenide semiconductors date back to the 1950s and have generated great interest because of their potential applications in optoelectronics and nonlinear optics.[1–6] Relative to binary II-VI chalcogenides, ternary I-III-VI$_2$ compounds can be generated through cross-substituting pairs of group I and III atoms for the group II atoms, with the octet rule still obeyed.[1,3] These ternary semiconductors exhibit more flexible properties arising from their enhanced chemical and structural freedoms.[7–11] For example, the band gap of CuGaSe$_2$ (1.68 eV), being lower than that of ZnSe (2.82 eV),[12] is more suitable for application in thin-film solar cells, especially when alloying with CuInSe$_2$ to lower the gap (close to the ideal 1.4 eV band gap for single junction solar cells).[13,14] Following this method, it is natural to further increase the chemical and structural freedoms to form novel quaternary chalcogenides, which have more functional and useful properties. In particular, the increased freedom will allow material scientists to tailor the chemical and physical properties to satisfy a certain requirement, e.g., for solar cell absorber layers or high-efficiency light emitting diodes.

Goodman[1] and Pamplin[3] pioneered the design of quaternary chalcogenides through cation cross-substitution in ternary I-III-VI$_2$ systems. While obeying the octet rule, there are two methods for this cation substitution: (i) to replace two group III atoms by one II and one IV atom, forming a I$_2$-II-IV-VI$_4$ compound; (ii) to replace one group I atom and one III by two II atoms, forming a I-III-II$_2$-VI$_4$ compound, which can also be taken as the II$_{2x}$(I-III)$_{1-x}$VI$_2$ alloy at x =0.5. Experimentally, such quaternary compounds with I

=Cu, Ag, II=Zn, Cd, III=Ga, In, IV=Ge, Sn, and VI=S, Se, Te have been synthesized by different groups.[4,6,15–18] Recently, significant attention has been paid to Cu$_2$ZnSnS$_4$ and Cu$_2$ZnSnSe$_4$ as absorber materials for thin-film solar cells[19–22] because they contain only abundant and nontoxic elements and their band gaps are reported to be around 1.5 eV. The binary-ternary alloys, such as Zn$_{2-2x}$(CuB)$_x$$X_2$ (B=Ga, In and X=S, Se, Te), are also studied for their applications in thin-film solar cells,[18,23] as well as Zn$_{2-2x}$(AgIn)$_x$S$_2$ in photocatalytic H$_2$ evolution from aqueous solutions (water splitting).[24]

As a result of the increased number of elements, quaternary chalcogenides have more structural configurations and more complicated electronic and structural properties than the binary and ternary ones. Unfortunately, quite limited theoretical attention has been paid to these systems,[25–27] hence the difference between different structural configurations and their inherent electronic structure trends are so far unclear, which limits their usage in semiconductor devices and future knowledge-based material design.

In this paper, we report a systematic investigation of the properties (crystal and electronic structures) of the binary, ternary, and quaternary chalcogenides from the cation substitution perspective to elucidate the underlying chemical trends. To demonstrate these trends clearly, we first limit cation substitution to the same elemental row in the periodic table (common-row cation substitution), e.g., Zn→CuGa →Cu$_2$ZnGe and Cd→AgIn→Ag$_2$CdGe in I$_2$-II-IV-VI$_4$, and Zn→CuGa→CuGaZn$_2$ and Cd→AgIn→AgInCd$_2$ in I-III-II$_2$-VI$_4$ systems, and then apply this understanding to other quaternary materials formed via cross-row cation substitution.

Our main findings may be summarized as follows. (i) For common-row-cation I_2-II-IV-VI$_4$ compounds, the low-energy kesterite (KS) structure, derived from the ternary chalcopyrite structure, has $\eta = \frac{c}{2a} < 1$, a negative crystal-field splitting, and the largest band gap. (ii) The valence-band offsets between II-VI and I_2-II-IV-VI$_4$ compounds are positive and large, while those between I-III-VI$_2$ and I_2-II-IV-VI$_4$ are always small, because the $p-d$ coupling between group I and VI cations raises the valence-band maximum (VBM) in both I-III-VI$_2$ and I_2-II-IV-VI$_4$ systems. (iii) The conduction-band minimum (CBM) level of I_2-II-IV-VI$_4$ is lower than that of I-III-VI$_2$ as a result of the lower cation s level of IV compared to III, which determines the band-gap decrease in the ternary to quaternary substitution. (iv) Similarly for the common-row-cation I-III-II$_2$-VI$_4$ compounds, the low-energy stannite (ST) structure is also derived from chalcopyrite and has $\eta = \frac{c}{2a} < 1$, a negative crystal-field splitting and the largest band gap. (v) Cross-row cation substitution from the ternary to quaternary chalcogenides shows more complicated trends in both the crystal structure and electronic band structure, depending on the relative sizes of the I, II, III, and IV elements. (vi) In comparison to the experimental literature, our analysis highlights a possible long-standing misunderstanding in the crystal structure determination of I_2-II-IV-VI$_4$ quaternary chalcogenides. We suggest that the widely assumed stannite structure reported in the literature for experimental samples is most likely a partially disordered kesterite structure.

II. CALCULATION METHODOLOGY

The electronic structure and total energies are calculated within the density-functional theory[28,29] formalism as implemented in the plane-wave code VASP.[30,31] For the exchange-correlation potential, we use the generalized gradient approximation (GGA) of Perdew and Wang (PW91).[32] The d states of group III and IV elements are treated explicitly as valence. The interaction between the core electrons and the valence electrons is included by the standard frozen-core projector augmented-wave potentials.[33] An energy cutoff of 300 eV was applied in all cases. For the Brillouin-zone integration, we used k-point meshes that are equivalent[34] to the $4 \times 4 \times 4$ Monkhorst-Pack meshes[35] for an eight-atom cubic unit cell. All lattice vectors and atomic positions were fully relaxed by minimizing the quantum-mechanical stresses and forces.

III. CRYSTAL STRUCTURES

It is well known that ternary I-III-VI$_2$ compounds (e.g., CuGaS$_2$) usually adopt the chalcopyrite (CH) structure (space group $I\bar{4}2d$) [Fig. 1(b)], in which the group VI atoms are surrounded by two group I and two III atoms, thus obeying the octet rule and forming a (I-VI)$_2$(III-VI)$_2$ (201) superlattice. Another metastable structure also obeying the octet rule and studied before[36,37] is the CuAu (CA)-like structure [Fig. 1(c)], which can be viewed both as a (I-VI)(III-VI) (001) superlattice and a (I-VI)(III-VI) (201) superlattice. It has been shown[36] that for consideration of total energies and
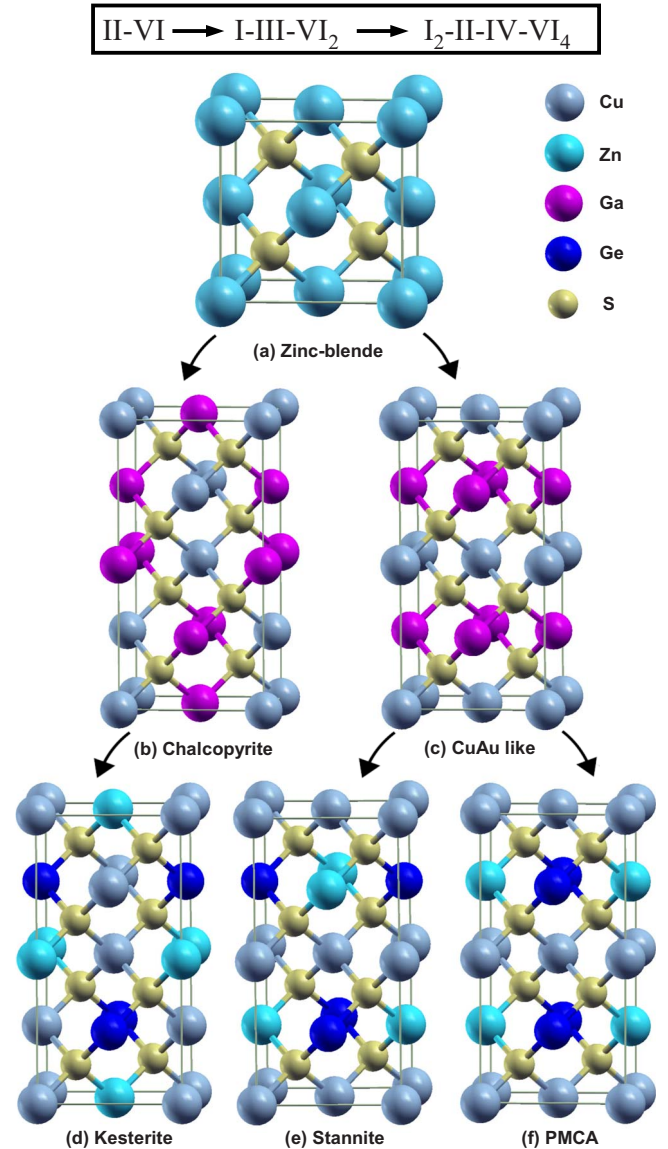

FIG. 1. (Color online) The crystal structure of (a) zinc-blende ZnS, (b) chalcopyrite CuGaS$_2$, (c) CuAu-like CuGaS$_2$, (d) KS-Cu$_2$ZnGeS$_4$, (e) ST-Cu$_2$ZnGeS$_4$, and (f) PMCA-Cu$_2$ZnGeS$_4$.

physical properties where the lowest pair interaction is dominant, the material properties of other configurations that satisfy the octet rule are bound between the CH and CA structures. Structures that do not obey the octet rule usually have much higher energy, thus they are not considered in this study.

When the group III cation is replaced by II and IV pairs in ternary chalcogenides, chalcopyrite I-III-VI$_2$ mutates exclusively into the KS-I_2-II-IV-VI$_4$ configuration (space group $I\bar{4}$, the Cu$_2$ZnSnS$_4$ structure[38]), a (I-VI)$_2$(II-VI)(IV-VI) (201) superlattice [Fig. 1(d)]. The replacement in CuAu-like I-III-VI$_2$ gives rise to two new quaternary configurations, ST (space group $I\bar{4}2m$, the Cu$_2$FeSnS$_4$ structure[38,39]), which is a (I-VI)(II-VI)(I-VI)(IV-VI) (201) superlattice [Fig. 1(e)], and the primitive-mixed CuAu structure (PMCA) (space group $P\bar{4}2m$) [Fig. 1(f)]. As in the ternary compounds, where the CA structure can be obtained from the CH structure by
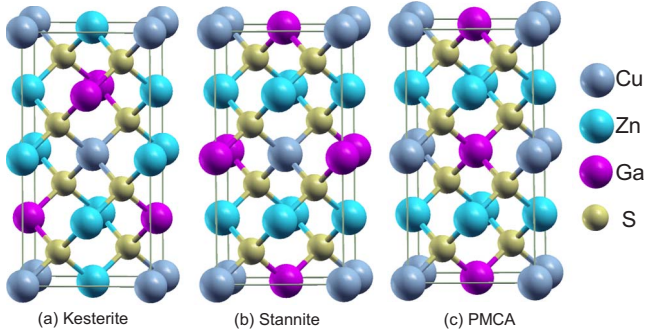
FIG. 2. (Color online) The crystal structure of (a) KS-CuGaZn$_2$S$_4$, (b) ST-CuGaZn$_2$S$_4$, and (c) PMCA-CuGaZn$_2$S$_4$.

switching atoms in every other two (001) planes,[36] the PMCA structure can also be obtained from the KS structure by switching atoms in every other two (001) planes. The ST structure can be obtained from the PMCA structures through exchange of the II and IV atoms in every other (II-IV) (001) plane and has a body-centered-tetragonal lattice vector as for KS, i.e., it has partial PMCA and partial KS character. All three quaternary configurations have eight-atom primitive cells, from which different superstructures that obey the octet rule can be constructed through alternative superposition of the three structures. Therefore, we expect that the total energies of KS and PMCA set limits for all other possible I$_2$-II-IV-VI$_4$ structural configurations.

Similarly for I-III-II$_2$-VI$_4$ materials, there are also three primitive-cell structures: (i) KS, a (I-VI)(III-VI)(II-VI)$_2$ (201) superlattice [Fig. 2(a)], (ii) ST, a (I-VI)(II-VI)(III-VI)(II-VI) (201) superlattice [Fig. 2(b)], and (iii) the PMCA structure [Fig. 2(c)]. Interestingly for this system, the ST structure can be obtained by replacing Cu and Ga by two Zn atoms in CH-I-III-VI$_2$, while the PMCA structure can be obtained from CA-I-III-VI$_2$ (with the c axis along the $\hat{x}$ direction). Here the KS structure has both CH and CA characters (i.e., one can obtain the KS structure from either CH or CA-I-III-VI$_2$ structures). Therefore, it is expected that, in this case, the ST and PMCA structures set total-energy limits for all other possible I-III-II$_2$-VI$_4$ structural configurations.

IV. II-VI TO I-III-VI$_2$ SUBSTITUTION

When II-VI chalcogenides mutate into I-III-VI$_2$ compounds, there are two fundamental I-III-VI$_2$ structures which obey the octet rule, the ground-state CH structure and metastable CA structure, from which all other structures obeying the octet rule can be constructed.[36] Consistent with previous observations,[7,37] our results demonstrate that the ternary chalcogenides always prefer the chalcopyrite structure, with an energy priority of about 10 meV for CH-CuGaS$_2$, CH-AgInS$_2$, and CH-CuGaSe$_2$ (Table I). In fact, the chalcopyrite structure is also the ground-state structure of many lattice-mismatched binary $A_{0.5}B_{0.5}C$ alloys under coherent conditions because it can accommodate the mismatched A-C and B-C bond lengths with lower strain energy[40] and also lower Madelung energy,[41] relative to the CuAu-like structure.

In contrast to the high-symmetry II-VI zinc-blende (ZB) structure, the ternary I-III-VI$_2$ compounds require three parameters to uniquely describe their crystal structure, the lattice constant a, the tetragonal lattice distortion parameter $\eta = \frac{c}{2a}$, and the anion displacement parameter $u = \frac{1}{4} + \frac{R_{\text{I-VI}}^2 - R_{\text{III-VI}}^2}{a^2}$, where $R_{\text{I-VI}}$ and $R_{\text{III-VI}}$ are the corresponding bond lengths. Comparing our calculated lattice constants and tetragonal distortion parameters for all ternary chalcogenides, we find that (i) the lattice constant a of the chalcopyrite structure is larger than that of CuAu-like structure and (ii) the tetragonal distortion parameter η is smaller than unity for the chalcopyrite structure, while larger than unity for the CuAu-like structure. This trend can be understood considering the different orientations of (I)$_2$(III)$_2$ clusters centered around the group VI atoms, e.g., in CuGaS$_2$, two Cu and two Ga atoms surround each S. In the CuAu structure, the Cu→S→Ga orientation is along the c axis, while in the chalcopyrite structure, it is along the a or b axis. When $R_{\text{I-VI}}$ and $R_{\text{III-VI}}$ differ, the group VI anions will displace from their ideal center and the resulting cluster is distorted from the ideal tetrahedron, e.g., elongating along the I→VI→III direction, while shrinking in the perpendicular plane. Then the basis vector of the CuAu structure along the c axis will be longer than those along a and b, giving $\eta > 1$, while the basis vector along c axis of chalcopyrite structure will be smaller than those along a and b, thus giving $\eta < 1$. A quantitative formula has been proposed to describe this relation, $\eta_{\text{CA}} = 2/(3\eta_{\text{CH}} - 1)$,[42] which our calculated results broadly follow.

As a result of the tetragonal symmetry, the ternary I-III-VI$_2$ compounds have a crystal-field splitting Δ_{CF} in the VBM, which is the energy-level difference between the doubly-degenerate Γ_{5v} states and the nondegenerate Γ_{4v} state.[9,43] According to our calculations, there is a clear trend in the crystal-field splitting: chalcogenides in the chalcopyrite structure have negative Δ_{cf} with $\eta < 1$, while the CuAu-like structure results in a positive Δ_{cf} with $\eta > 1$ (Table I). This is consistent with the fact that for all the ZB semiconductors, the [001] tetragonal deformation potential of the VBM state is negative.[12,44] It should be noted that the cross-row-cation CH-CuInSe$_2$ (and similarly CuInS$_2$) has a slightly positive $\Delta_{CF} = 0.0038$ meV and $\eta = 1.0048$,[45,46] different from most of other I-III-VI$_2$ chalcopyrites which have negative Δ_{CF} and $\eta < 1$,[12] which was studied by Wei and Zunger.[8,47] For CH-CuInSe$_2$, the sign of the crystal-field splitting is very sensitive to the structural parameters, but it is safe to say that it is small, close to zero.

One obvious electronic change in the substitution from the binary to ternary chalcogenides is the band-gap decrease of the ground-state structures. For example, from ZnS to CH-CuGaS$_2$, the calculated GGA band gap decreases from 2.01 to 0.69 eV (Table I). As we know, GGA usually underestimates the band gap, so our calculated value is significantly lower than the corresponding experimental value; however, the band-gap difference between the binary and the corresponding ternary is well estimated, which means the error between the GGA calculated and experimental band gaps is almost the same for the corresponding chalcogenides. For example, the gap error is 1.77 eV for ZnS, close to 1.74 eV for CuGaS$_2$; the band-gap error is 1.57 eV for CdS, close

TABLE I. Calculated lattice constant, tetragonal distortion parameter, crystal-field splitting, GGA direct band gap, GGA-corrected direct band gap, available experimental band gap, and the energy difference per atom relative to the lowest-energy structure of different chalcogenides.

Structure	a (Å)	η	Δ_{cf} (eV)	E_g^{GGA} (eV)	E_g^{th} (eV)	E_g^{exp} (eV)	ΔE (meV)
ZnS	5.441	1	0	2.01	3.78	3.78	0
CH-CuGaS$_2$	5.370	0.991	−0.12	0.69	2.43	2.43	0
CA-CuGaS$_2$	5.316	1.017	0.36	0.41	2.15		10.09
KS-Cu$_2$ZnGeS$_4$	5.358	0.993	−0.09	0.53	2.27		0
ST-Cu$_2$ZnGeS$_4$	5.333	1.007	0.29	0.32	2.06		4.69
PMCA-Cu$_2$ZnGeS$_4$	5.334	1.009	0.27	0.20	1.94		12.73
ZnSe	5.718	1	0	1.17	2.82	2.82	0
CH-CuGaSe$_2$	5.670	0.993	−0.10	0.03	1.68	1.68	0
CA-CuGaSe$_2$	5.616	1.009	0.21	−0.19	1.46		11.13
KS-Cu$_2$ZnGeSe$_4$	5.672	0.993	−0.07	−0.15	1.50	1.518	0
ST-Cu$_2$ZnGeSe$_4$	5.652	1.003	0.15	−0.33	1.32		4.88
PMCA-Cu$_2$ZnGeSe$_4$	5.643	1.006	0.15	−0.44	1.21		10.72
ZnTe	6.167	1	0	1.09	2.39	2.39	
CH-CuGaTe$_2$	6.071	0.998	−0.04	0.24	1.23	1.23	
KS-Cu$_2$ZnGeTe$_4$	6.065	0.997	−0.02	−0.18	0.81		
CdS	5.992	1	0	1.03	2.60	2.6	0
CH-AgInS$_2$	5.925	0.968	−0.17	0.34	1.87	1.87	0
CA-AgInS$_2$	5.747	1.058	0.42	0.19	1.72		10.28
KS-Ag$_2$CdSnS$_4$	5.912	0.976	−0.12	0.33	1.86		0
ST-Ag$_2$CdSnS$_4$	5.800	1.032	0.31	0.19	1.72		6.16
PMCA-Ag$_2$CdSnS$_4$	5.797	1.034	0.30	0.20	1.74		12.65
CdSe	6.196	1	0	0.48	1.74	1.74	
CH-AgInSe$_2$	6.196	0.971	−0.15	−0.10	1.24	1.24	
KS-Ag$_2$CdSnSe$_4$	6.179	0.980	−0.10	−0.14	1.20		
CdTe	6.609	1	0	0.59	1.48	1.48	
CH-AgInTe$_2$	6.559	0.990	−0.08	0.06	0.96	0.96	
KS-Ag$_2$CdSnTe$_4$	6.554	0.990	−0.05	−0.11	0.79		

to 1.53 eV for AgInS$_2$. To more readily compare to experiment, we have corrected the GGA calculated band gaps for each quaternary chalcogenide using the band-gap error of the corresponding ternary chalcogenide, for example, the corrected band gap for KS-Cu$_2$ZnGeS$_4$ is 2.27 eV, which is the calculated value 0.53 eV plus the gap error 1.74 eV of CH-CuGaS$_2$. The corrected band gaps show good agreement with the experimental values, for example, the corrected gap is 1.50 eV for KS-Cu$_2$ZnGeSe$_4$, close to the experimental value of 1.52 eV of Lee and Kim,[17] and the corrected and experimental values are 1.64 and 1.5 eV (Ref. [48]), respectively, for Cu$_2$ZnSnS$_4$ and 2.04 and 2.05 eV (Ref. [49]) for Cu$_2$CdGeS$_4$. Considering the experimental uncertainty, our correction is expected to be reliable within 0.15 eV.

In the ternary CH-CuGaS$_2$ system, the decrease of the band gap relative to ZnS is previously well studied and attributed to the VBM upshift caused by the $p−d$ coupling between Cu and S, as well as the CBM downward shift caused by the low s level of Ga (Table [II]).[7,9] This can be seen clearly in the band alignments between ZnS and CH-CuGaS$_2$ (Fig. [3]) and has also been empirically proved in recent experiment on the corresponding selenides.[50]

TABLE II. Calculated atomic valence orbital energies ϵ_s, ϵ_p, and ϵ_d (in eV) of related elements. The all-electron calculations are performed using the local-density approximation within density-functional theory.

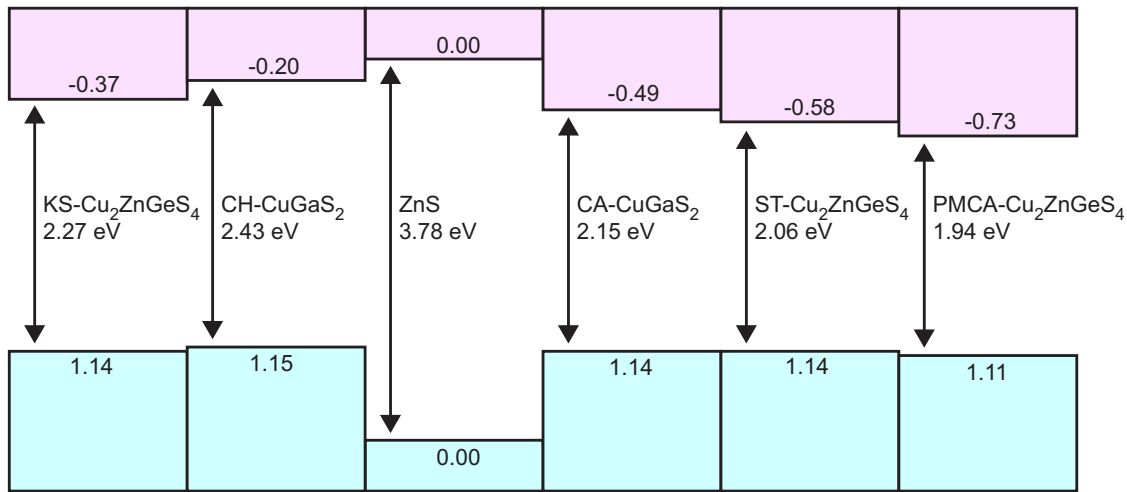| Atom	ϵ_s	ϵ_p	ϵ_d
Cu	−4.95		−5.39
Zn	−6.31	−1.31	−10.49
Ga	−9.25	−2.82	−19.18
Ge	−12.03	−4.14	−29.58
Ag	−4.80		−7.73
Cd	−6.04	−1.41	−11.96
In	−8.55	−2.78	−18.75
Sn	−10.89	−3.96	−25.93
S	−17.36	−7.19	
Se	−17.56	−6.74	−53.45
Te	−15.44	−6.20	−41.77

FIG. 3. (Color online) The calculated band alignment of ZnS, $CuGaS_2$, and Cu_2ZnGeS_4.

Compared to the ground-state chalcopyrite structure, the metastable CA-I-III-VI_2 compounds always have a smaller direct band gap at the Γ point, which is due to the Γ(ZB) and X_z(ZB) coupling that is not allowed in the CH structure but allowed in CA structure. According to our calculation, their valence-band offset is very small, e.g., only 0.01 eV between CH-$CuGaS_2$ and CA-$CuGaS_2$, showing that the Γ(ZB) and X_z(ZB) coupling in the VBM state is negligible and thus the gap difference is contributed mainly by the CBM downshift.

V. I-III-VI_2 TO I_2-II-IV-VI_4 SUBSTITUTION

A. Total energy and lattice distortion

As the ternary I-III-VI_2 chalcogenides mutate further into the quaternary I_2-II-IV-VI_4 system, we found that the CH-derived KS structure is the ground state for Cu_2ZnGeS_4, Ag_2CdSnS_4, and $Cu_2ZnGeSe_4$, while the PMCA structure has the highest energy and the ST structure is in between. This energy priority can be understood from the underlying structural derivation relationships. As we know, CH has lower energy than CA for ternary I-III-VI_2 because it has lower strain and Madelung energy. In the common-row cation substitution, the group III atom is replaced by the neighboring II and IV atoms. As the change in the cation sizes is small, KS has similar strain energy to CH, lower than those of both ST and PMCA which are derived from the CA structure. Similarly, our calculations reveal that the Madelung energy increases in the order of KS, ST, and PMCA, consistent with our expectation. Combining the effect of strain and Madelung energy, we obtain that the total energy increases in the order KS, ST, and PMCA, which should be valid for all the common-row cation substitution systems. Based on this observation we calculated only the properties of the ground-state KS structure for the $Cu_2ZnGeTe_4$, $Ag_2CdSnSe_4$, and $Ag_2CdSnTe_4$ systems.

The inheritance relations also influence the lattice parameters of the quaternary chalcogenides. Like in the ternary systems, for the quaternary I_2-II-IV-VI_4, the CH-derived KS structure also has larger a, smaller η, and hence more negative Δ_{CF} than the CuAu-derived ST and PMCA structures

(Table I). For example, the values for KS-Cu_2ZnGeS_4 are 5.358 Å, 0.993, and -0.088 eV, respectively, and for ST-Cu_2ZnGeS_4 are 5.333 Å, 1.007, and 0.289 eV. This is easy to understand for common-row cation substitutions since Zn and Ge have atomic numbers close to Ga and therefore their size and chemical differences are small, making the previous explanation for the ternary compounds also apply here. We find that in the substitution process from binary to ternary to quaternary, the change in the lattice constants is very small. This makes these materials and their alloys potential candidates for producing high efficiency tandem solar cells providing strong optical absorption and efficient doping can be achieved.

B. Band structure and valence-band offset

It is one of the major goals in this study to understand how the band structure of chalcogenides changes through cation cross-substitution. The calculated results for common-row I_2-II-IV-VI_4 compounds are shown in Table I. We find that all the ground-state KS quaternary chalcogenides have a lower band gap than the corresponding ternary chalcopyrites. For example, KS-Cu_2ZnGeS_4 has a GGA-corrected direct gap of 2.27 eV, 0.16 eV lower than that of CH-$CuGaS_2$. Since in the further substitution from $CuGaS_2$ to Cu_2ZnGeS_4, only Ga is replaced by Zn and Ge, while the VBM state arises mostly from Cu-S p-d coupling due to the low binding energy of the Cu d level (Table II). We expect that the band-gap decrease in the quaternary compounds should be mainly caused by the downshift of the CBM.

To check the influence of the VBM, we calculated the valence-band offsets[8,9,11] between each pair of mutated compounds in their ground-state structures (Table III). According to these results, the valence-band offsets between ZnS and CH-$CuGaS_2$ or KS-Cu_2ZnGeS_4 are both large and positive, but that between KS-Cu_2ZnGeS_4 and CH-$CuGaS_2$ is very small (Fig. 3). This is because the VBM levels are dominated by Cu d and S p orbitals (Fig. 4). The valence-band offsets between other binary and their corresponding ternary or quaternary chalcogenides follow the same trend as the ZnS sys-

TABLE III. The calculated valence-band offset (in eV) for the chalcogenides studied in the present paper. Effects of spin-orbit splitting are not included because they are small for the common-anion systems studied here.

$ZnS/CH\text{-}CuGaS_2$	$CH\text{-}CuGaS_2/KS\text{-}Cu_2ZnGeS_4$	$ZnS/KS\text{-}Cu_2ZnGeS_4$
1.15	−0.02	1.13
$ZnSe/CH\text{-}CuGaSe_2$	$CH\text{-}CuGaSe_2/KS\text{-}Cu_2ZnGeSe_4$	$ZnSe/KS\text{-}Cu_2ZnGeSe_4$
0.86	−0.02	0.84
$ZnTe/CH\text{-}CuGaTe_2$	$CH\text{-}CuGaTe_2/KS\text{-}Cu_2ZnGeTe_4$	$ZnTe/KS\text{-}Cu_2ZnGeTe_4$
0.57	0.05	0.62
$CdS/CH\text{-}AgInS_2$	$CH\text{-}AgInS_2/KS\text{-}Ag_2CdSnS_4$	$CdS/KS\text{-}Ag_2CdSnS_4$
0.61	−0.01	0.60
$CdSe/CH\text{-}AgInSe_2$	$CH\text{-}AgInSe_2/KS\text{-}Ag_2CdSnSe_4$	$CdSe/KS\text{-}Ag_2CdSnSe_4$
0.52	−0.03	0.49
$CdTe/CH\text{-}AgInTe_2$	$CH\text{-}AgInTe_2/KS\text{-}Ag_2CdSnTe_4$	$CdTe/KS\text{-}Ag_2CdSnTe_4$
0.35	0.10	0.45

tems, showing that in the substitution, the $p-d$ coupling between I and VI atoms always determines the VBM level and is weakly related to the II, III, and IV atoms. This $p-d$ coupling decreases as the bond lengths between the I-IV pairs increase. This explains the decrease in offsets between the binary and the corresponding ternary or quaternary chalcogenides as the size of the anions increases, e.g., the offset for $CdS/CH\text{-}AgInS_2$ is 0.57 eV and for $CdTe/CH\text{-}AgInTe_2$ is 0.35 eV.

Since the decrease of band gap is governed by the CBM downshift produced in the substitution from Ga to Zn and Ge (see Fig. 3), we will investigate how Zn and Ge determine this shift. Charge density plots arising from the $KS\text{-}Cu_2ZnGeS_4$ band extrema are shown in Fig. 4. These show that the CBM state is localized mainly on Ge and S, while the VBM state is localized mainly on Cu and S. Further band component analysis indicates that the CBM state is a Ge s and S s and p hybrid orbital. Relative to Ga in $CH\text{-}CuGaS_2$, Ge in the quaternary $KS\text{-}Cu_2ZnGeS_4$ has a lower s level (Table II), therefore, Ge-S hybridization produces a lower antibonding level in the CBM than Ga-S, which explains the obvious band-gap decrease from ternary $CH\text{-}CuGaS_2$ to quaternary $KS\text{-}Cu_2ZnGeS_4$. Similarly for $Ag_2CdSn\text{-}VI_4$ and other selenide and telluride quaternaries, the lower s level of IV atoms compared to III atoms determines the downshift of the CBM and hence the decrease in the band gap (Table II).
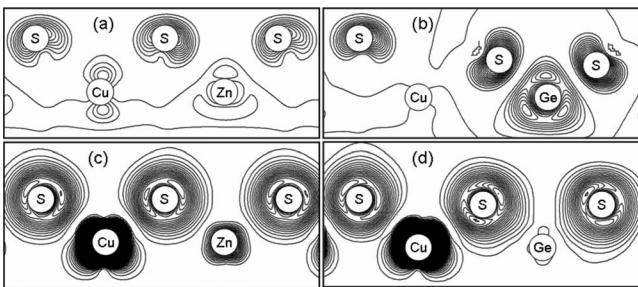

FIG. 4. Charge density plots of the $KS\text{-}Cu_2ZnGeS_4$ CBM in the (a) Cu-S-Zn plane and (b) Cu-S-Ge plane, and the VBM in the (c) Cu-S-Zn plane and (d) Cu-S-Ge plane.

Like in the ternary case, the direct gaps at the Γ point of $I_2\text{-}II\text{-}IV\text{-}VI_4$ in the CA-derived ST and PMCA structures are also smaller than those of the CH-derived KS structures (Table I). As we can see from the valence-band offset (Fig. 3), the differences between the VBM of CH and CA-derived structures are quite small, so it is again the CBM downshift that has the strongest influence.

Band structures for the three quaternary phases of Cu_2ZnGeS_4 are shown along the $T(Z) \rightarrow \Gamma \rightarrow N(A)$ lines in Fig. 5. The fundamental gap of $PMCA\text{-}Cu_2ZnGeS_4$ becomes indirect, with the CBM at A and the VBM at Γ, while the gaps of $KS\text{-}Cu_2ZnGeS_4$ and $ST\text{-}Cu_2ZnGeS_4$ are both direct at the Γ point. The upper valence band of $PMCA\text{-}Cu_2ZnGeS_4$ and $ST\text{-}Cu_2ZnGeS_4$ are similar; however, the conduction band of $PMCA\text{-}Cu_2ZnGeS_4$ from Γ to A changes dramatically, with the CBM state located at the A point. This is because in the PMCA structure, the low conduction bands of Cu_2ZnGeS_4 at the A point have three segregating states:[51] one doubly-degenerate state localized on CuS, one single-degenerate state localized on ZnS, and one
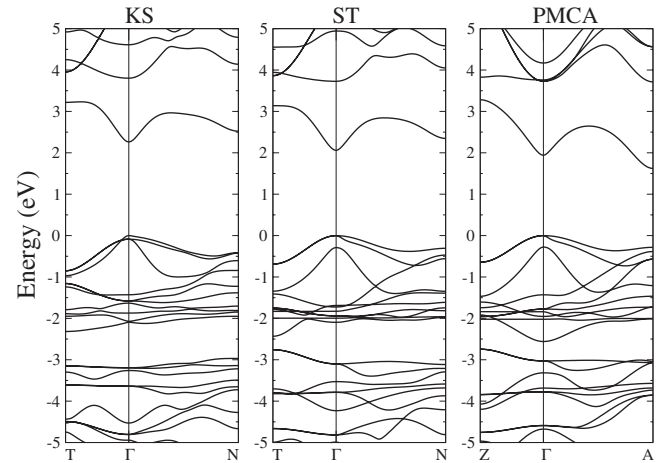

FIG. 5. The GGA-corrected band structure along the high-symmetry lines, $T(Z): \frac{2\pi}{a}(0\ 0\ 0.5) \rightarrow \Gamma: (0\ 0\ 0) \rightarrow N(A): \frac{2\pi}{a}(0.5\ 0.5\ 0.5)$, in the first Brillouin zone for (a) $KS\text{-}Cu_2ZnGeS_4$, (b) $ST\text{-}Cu_2ZnGeS_4$, and (c) $PMCA\text{-}Cu_2ZnGeS_4$.

TABLE IV. Calculated lattice constant, tetragonal distortion parameter, crystal-field splitting, GGA direct band gap, GGA-corrected direct band gap, and energy difference per atom relative to the lowest-energy structure of I-III-II$_2$-VI$_4$ chalcogenides.

Compounds	a (Å)	η	Δ_{cf} (eV)	E_g^{GGA} (eV)	E_g^{th} (eV)	ΔE (meV)
KS-CuGaZn$_2$S$_4$	5.392	1.003	0.09	1.06	2.82	2.38
ST-CuGaZn$_2$S$_4$	5.406	0.995	−0.07	1.15	2.91	0
PMCA-CuGaZn$_2$S$_4$	5.405	0.994	−0.14	0.90	2.66	5.33
KS-CuGaZn$_2$Se$_4$	5.689	1.002	0.05	0.35	2.00	2.44
ST-CuGaZn$_2$Se$_4$	5.701	0.995	−0.07	0.45	2.10	0
PMCA-CuGaZn$_2$Se$_4$	5.702	0.995	−0.09	0.21	1.86	5.55
KS-AgInCd$_2$S$_4$	5.884	1.004	0.07	0.59	2.14	3.20
ST-AgInCd$_2$S$_4$	5.919	0.987	−0.10	0.63	2.18	0
PMCA-AgInCd$_2$S$_4$	5.895	0.997	−0.09	0.46	2.01	7.09
KS-AgInCd$_2$Se$_4$	6.158	1.004	0.05	0.11	1.41	3.01
ST-AgInCd$_2$Se$_4$	6.185	0.991	−0.07	0.15	1.45	0
PMCA-AgInCd$_2$Se$_4$	6.194	0.987	−0.10	0	1.30	6.13

single-degenerate state arising from GeS, which is the CBM due to the much lower Ge s energy level. At Γ, the same analysis shows that although Ge and S components dominate the lowest conduction-band state, Cu and Zn also have a weak contribution; therefore, the energy level is higher than at the A point and the system becomes indirect.

C. Comparison to experiment

Comparing our calculations to available experimental results, we notice that many of the literature reports on I$_2$-II-IV-VI$_4$ compounds claim that the synthesized samples crystallize in the stannite structure.[4,6,15–17,52–54] For example, Parasyuk and co-workers synthesized Cu$_2$ZnGeS$_4$ and Cu$_2$ZnGeSe$_4$ samples from high-purity components and determined their crystal structure by x-ray powder diffraction.[15,16] They claim both samples crystallized in the ST structure with a=5.3413 Å and η=0.9838 for Cu$_2$ZnGeS$_4$ and a=5.6104 Å and η=0.9844 for Cu$_2$ZnGeSe$_4$. Our calculated structural parameters show that only the KS structure has η less than unity and has lower energy than the stannite structure. We believe that the discrepancy between our calculation and experimental assignment is caused by the fact that due to the similarity between Cu and Zn, cation disorder in the Cu+Zn layer of KS structure can easily occur. As we can see in Fig. 1(d), the KS structure has an ordering of cations in the (001) planes, which can be expressed as repeating layers of /Cu+Zn/Cu +Ge/Zn+Cu/Ge+Cu/. In a supercell of the KS structure, if Zn and Cu in some of the Cu+Zn layers are exchanged, i.e., the atoms in the layers are shifted by $\langle\frac{1}{2},\frac{1}{2},0\rangle a$. This new structure still obeys the octet rule, so the total-energy change is very small, which is confirmed by our calculation. If the displacement occurs randomly in the Cu+Zn layers, it gives an effective symmetry equivalent to the stannite structure. Experimentally, because the atomic numbers of Cu, Zn, and Ge are close, it is very difficult to detect the cation disorder using x-ray diffraction. Therefore, we propose that it is most likely that the partially disordered KS structures may have been synthesized in previous experiments rather than the claimed ST structure.[15,16] In fact, the partially disordered KS structure was observed in a recent neutron-diffraction experiment for Cu$_2$ZnSnS$_4$.[55]

Another experimental study of Cu$_2$ZnGeSe$_4$ was performed by Lee and Kim[17] and found a=5.618 Å and η =0.9826. The direct band gap of 1.518 eV, determined from the optical-absorption spectra, is significantly larger than the band gap of 1.29 eV reported by Schleich and Wold[6] for Cu$_2$ZnGeSe$_4$ single crystals. According to our predictions, the GGA-corrected band gaps of Cu$_2$ZnGeSe$_4$ can vary between 1.21 to 1.50 eV, depending on different atomic configurations. The band gap can be reduced further by the partial disorder in the Cu+Zn layer. Therefore, we suggest that Lee and Kim[17] synthesized more ideal KS-Cu$_2$ZnGeSe$_4$ crystals, whereas the Cu$_2$ZnGeSe$_4$ samples grown by Schleich and Wold[6] may contain more disordered or mixed structures. More experimental investigations are needed to test our predictions.

VI. II-VI/I-III-VI$_2$ ALLOY

The I-III-II$_2$-VI$_4$ chalcogenides, as an alloy of II-VI and I-III-VI$_2$ compounds, have different cation distributions around the group VI anions from the I$_2$-II-IV-VI$_4$ systems; however, some trends in their crystal and electronic structures are similar. It should be kept in mind that for this case, ST ordering is derived from the ternary CH structure, PMCA ordering is derived from the ternary CA structure, while KS can be derived from both CH or CA structures. As Table IV shows, the ST phase is always the ground-state structure when one group I atom and one group III atom are replaced by two group II atoms in the same row of the periodic table. Furthermore, the established trends in the lattice distortion, crystal-field splitting, and band gap all exist in this system as

TABLE V. Calculated lowest-energy structure, lattice constant, tetragonal distortion parameter, crystal-field splitting, GGA direct band gap, and GGA-corrected direct band gap of the cross-row-substitution I_2-II-IV-VI_4 and I-III-II_2-VI_4 chalcogenides.

Compounds	a (Å)	η	Δ_{cf} (eV)	E_g^{GGA} (eV)	E_g^{th} (eV)
KS-Cu_2ZnSnS_4	5.467	0.999	−0.07	0.09	1.64
ST-Cu_2CdGeS_4	5.532	0.964	0.04	0.30	2.04
ST-Cu_2CdSnS_4	5.616	0.983	0.00	−0.05	1.50
KS-Ag_2ZnSnS_4	5.841	0.945	−0.20	0.45	1.98
KS-Ag_2CdGeS_4	5.825	0.957	−0.09	0.71	2.41
KS-Ag_2ZnGeS_4	5.762	0.921	−0.21	0.86	2.56
KS-$CuGaCd_2S_4$	5.662	0.984	0.09	0.51	2.17
KS-$AgInZn_2S_4$	5.648	0.995	0.06	0.90	2.55
KS-$CuInZn_2S_4$	5.514	0.999	−0.02	0.68	2.34
KS-$CuInCd_2S_4$	5.762	0.995	0.02	0.22	1.78
ST-$AgGaZn_2S_4$	5.595	0.963	−0.05	1.39	3.13
ST-$AgGaCd_2S_4$	5.855	0.959	−0.18	0.90	2.54

in I_2-II-IV-VI_4, i.e., (i) a is larger and η smaller, (ii) Δ_{cf} is negative, and (iii) the band gap is larger in the CH-derived ST structure. The PMCA structure always has the highest total energy and smallest band gap, whereas the KS structure is in between, as expected. However, the energy differences between the structures are small in the I-III-II_2-VI_4 chalcogenides, which indicates a higher possibility of forming mixed superstructures.

Comparing the band gaps of II-VI and I-III-VI_2 composites, the gaps of the I-III-II_2-VI_4 alloys are always larger than those of the I-III-VI_2 components, while lower than their ideal average, giving a positive bowing parameter. The GGA-corrected value is 2.91 eV for ST-$CuGaZn_2S_4$, between 3.78 eV (ZnS) and 2.43 eV (CH-$CuGaS_2$). As we know, there are large valence and conduction-band offsets between ZnS and CH-$CuGaS_2$, so the band-gap change of the I-III-II_2-VI_4 alloy relative to the two composites results from shifts in both the VBM and CBM states.

VII. CROSS-ROW SUBSTITUTION

Our previous discussions were limited to common-row substitutions in order to extract the basic chemical trends from the quaternary I_2-II-IV-VI_4 and I-III-II_2-VI_4 chalcogenides. These were shown to be consistent with the corresponding trends in the ternary I-III-VI_2 chalcogenides. On consideration of cross-row substitutions, the trends become more complicated and depend sensitively on the relative sizes of the group I, II, III, and IV elements and their chemical bonding behaviors. Here, the quaternary ground-state structure may be either KS or ST, with the PMCA structure always higher in total energy (Table V). This is because in the cross-row cation substitution, the strain energy depends sensitively on the bond-length-mismatch, breaking the expectation that CH-derived structures have lower strain energy than CA-derived structures. Despite these complications, our earlier observations still hold some weight: no matter which structure is adopted as the ground state, that

structure always has a larger a and a tetragonal distortion parameter $\eta = c/2a$ smaller than unity. For these systems, it should be noted that the crystal-field splitting is not always negative in the ground-state structure as for the common-row substitutions.

To understand how the size difference of cations (bond-length mismatch) influences the total-energy difference between KS and ST structures $\Delta E_{\text{ST-KS}}$ and their crystal-field splitting Δ_{cf}, we performed a three-step calculation for the representative Cu_2CdGeS_4 and $CuGaCd_2S_4$, according to the theoretical work of Rowe and Shay,[43] which extends the quasicubic model to ternary chalcopyrite crystals. They pointed out that there are three contributions to the noncubic crystal field: (a) the ordering of the different metal cations Δ_{ord}, (b) the anion displacement from the ideal zinc-blende site Δ_{dis}, and (c) the tetragonal distortion Δ_{str}. In our study we analyze the three contributions through a three-step calculation: (A) all cations and anions are located at ideal zinc-blende sites and the cell is fixed cubic with no distortion. The calculated Δ_{cf} equals to Δ_{ord}, because only the chemical differences of the cations influence the splitting. (B) following step A, the atomic positions are relaxed while the cell is still kept cubic and the change of Δ_{cf} equals to Δ_{dis} because only anions are displaced from ideal zinc-blende sites as a result of the crystal symmetry. (C) the cell is allowed for relaxation and the change gives Δ_{str}. In the step A and B, the volume of unit cell are set to be equal to the equilibrium volume. The results are listed in Table VI. We found that (i) without a relaxation of the bond length (step A), the total energy of CH-derived KS-Cu_2CdGeS_4 is lower than that of CA-derived ST-Cu_2CdGeS_4, like in the case of common-row-cation I_2-II-IV-VI_4 compounds which have small bond-length mismatch. However, after the atomic position relaxation, the trend is reversed, i.e., the energy of KS-Cu_2CdGeS_4 is now higher than ST-Cu_2CdGeS_4, indicating the large contribution of the bond-length mismatch to $\Delta E_{\text{ST-KS}}$. For $CuGaCd_2S_4$, the ST structure has lower energy than the KS structure before relaxation, like in common-row-cation I-III-II_2-VI_4, but ST structure has higher energy than KS structure after relax-

TABLE VI. With different degrees (A, B, C) for the structural relaxation, the calculated η, Δ_{cf}, and direct band gaps of Cu_2CdGeS_4 and $CuGaCd_2S_4$ in ST and KS structures, respectively, and their total-energy difference per atom $\Delta E_{\text{ST-KS}}$.

	η	Δ_{cf} (eV)	E_g^{GGA} (eV)	η	Δ_{cf} (eV)	E_g^{GGA} (eV)	$\Delta E_{\text{ST-KS}}$ (meV)
	KS-Cu_2CdGeS_4			ST-Cu_2CdGeS_4			
A	1	−0.06	0.09	1	0.21	−0.03	5.68
B	1	0.02	0.35	1	0.13	0.28	−10.01
C	1.007	0.03	0.34	0.964	0.04	0.30	−12.70
	KS-$CuGaCd_2S_4$			ST-$CuGaCd_2S_4$			
A	1	0.07	0.38	1	−0.06	0.45	−2.78
B	1	0.13	0.49	1	−0.14	0.53	12.00
C	0.984	0.09	0.51	1.011	−0.12	0.53	12.29

ation. (ii) Before structural relaxation, the CA-derived structures for both compounds (ST-Cu_2CdGeS_4, KS-$CuGaCd_2S_4$) have positive Δ_{cf} and CH-derived structures (KS-Cu_2CdGeS_4, ST-$CuGaCd_2S_4$) have negative Δ_{cf}. The structural relaxation has significant contribution to Δ_{cf}, as large as 0.17 eV for ST-Cu_2CdGeS_4 and changing the sign of Δ_{cf} for KS-Cu_2CdGeS_4. The change due to the tetragonal distortion (steps B and C, Δ_{str}) has the same sign as $\eta-1$, consistent with the negative [001] tetragonal deformation potential of the VBM state for all the ZB semiconductors.[12,44]

Comparing to ternary chalcogenides, which all have negative or small positive crystal-field splitting in their ground-state CH structure, the quaternary chalcogenides mixed in characters of the metastable CA structure. The diversity of these cross-row quaternary chalcogenides indicates that some novel functionalities and applications may arise.

VIII. CONCLUSION

In conclusion, using first-principles calculations, a series of binary (II-VI), ternary (I-III-VI_2), and quaternary (I$_2$-II-IV-VI_4 and I-III-II$_2$-VI_4) chalcogenides has been studied from a cation cross-substitution perspective. From our analysis, we identify common trends in the crystal and electronic structures of these multiternary chalcogenides when their cations are in the same elemental row of the periodic table. We also find that in the two-step cross-substitution from binary to quaternary, the VBM states remain dominated by the antibonding $p-d$ coupling between the group I and VI atoms, while CBM states are influenced by the antibonding coupling between the group III or IV s state and VI s and p states. In the cross-substitution from ternary to quaternary, the VBM level shifts very little and the band-gap decrease arises mainly through the significant CBM downshift. In comparison to experiment, our results show that there may be a long-standing misunderstanding in the crystal structure determination of the I$_2$-II-IV-VI_4 quaternary chalcogenides, which becomes important for the accurate characterization of the chemical and physical properties and hence their application in future optoelectronic devices.

[1] C. H. L. Goodman, J. Phys. Chem. Solids **6**, 305 (1958).

[2] B. R. Pamplin, Nature (London) **188**, 136 (1960).

[3] B. R. Pamplin, J. Phys. Chem. Solids **25**, 675 (1964).

[4] H. Hahn and H. Schulze, Naturwiss. **52**, 426 (1965).

[5] R. Nitsche, D. F. Sargent, and P. Wild, J. Cryst. Growth **1**, 52 (1967).

[6] D. M. Schleich and A. Wold, Mater. Res. Bull. **12**, 111 (1977).

[7] J. E. Jaffe and A. Zunger, Phys. Rev. B **28**, 5822 (1983).

[8] S.-H. Wei and A. Zunger, J. Appl. Phys. **78**, 3846 (1995).

[9] S. Chen, X. G. Gong, and S.-H. Wei, Phys. Rev. B **75**, 205209 (2007).

[10] A. Walsh and S.-H. Wei, Phys. Rev. B **76**, 195208 (2007).

[11] Y. Z. Zhu, G. D. Chen, H. Ye, A. Walsh, C. Y. Moon, and S.-H. Wei, Phys. Rev. B **77**, 245209 (2008).

[12] O. M. Madelung, *Semiconductors: Data Handbook*, 3rd ed. (Springer, New York, 2004).

[13] M. A. Green, K. Emery, Y. Hisikawa, and W. Warta, Prog. Photovoltaics **15**, 425 (2007).

[14] J. D. Beach and B. E. McCandless, MRS Bull. **32**, 225 (2007).

[15] O. V. Parasyuk, L. D. Gulay, Y. E. Romanyuk, and L. V. Piskach, J. Alloys Compd. **329**, 202 (2001).

[16] O. V. Parasyuk, L. V. Piskach, Y. E. Romanyuk, I. D. Olekseyuk, V. I. Zaremba, and V. I. Pekhnyo, J. Alloys Compd. **397**, 85 (2005).

[17] C. Lee and C.-D. Kim, J. Korean Phys. Soc. **37**, 364 (2000).

[18] S. Schorr, G. Wagner, M. Tovar, and D. Sheptyakov, Mater. Res. Soc. Symp. Proc. **1012**, Y03-05 (2007).

[19] H. Katagiri, Thin Solid Films **480-481**, 426 (2005).

[20] J. J. Scragg, P. J. Dale, L. M. Peter, G. Zoppi, and I. Forbes, Phys. Status Solidi B **245**, 1772 (2008).

[21] K. Moriya, K. Tanaka, and H. Uchiki, Jpn. J. Appl. Phys. **47**, 602 (2008).

[22] M. Altosaar, J. Raudoja, K. Timmo, M. Danilson, M. Grossberg, J. Krustok, and E. Mellikov, Phys. Status Solidi A **205**, 167 (2008).

[23] S. Schorr, V. Riede, D. Spemann, and T. Doering, J. Alloys Compd. **414**, 26 (2006).

[24] I. Tsuji, H. Kato, H. Kobayashi, and A. Kudo, J. Am. Chem. Soc. **126**, 13406 (2004).

[25] R. Osorio, Z. W. Lu, S.-H. Wei, and A. Zunger, Phys. Rev. B **47**, 9985 (1993).

[26] J. M. Raulot, C. Domain, and J. F. Guillemoles, J. Phys. Chem. Solids **66**, 2019 (2005).

[27] S. Chen, X. G. Gong, A. Walsh, and S.-H. Wei, Appl. Phys. Lett. **94**, 041903 (2009).

[28] W. Kohn and L. J. Sham, Phys. Rev. **140**, A1133 (1965).

[29] P. Hohenberg and W. Kohn, Phys. Rev. **136**, B864 (1964).

[30] G. Kresse and J. Furthmüller, Phys. Rev. B **54**, 11169 (1996).

[31] G. Kresse and J. Furthmüller, Comput. Mater. Sci. **6**, 15 (1996).

[32] J. P. Perdew, J. A. Chevary, S. H. Vosko, K. A. Jackson, M. R. Pederson, D. J. Singh, and C. Fiolhais, Phys. Rev. B **46**, 6671 (1992).

[33] G. Kresse and D. Joubert, Phys. Rev. B **59**, 1758 (1999).

[34] S. Froyen, Phys. Rev. B **39**, 3168 (1989).

[35] H. J. Monkhorst and J. D. Pack, Phys. Rev. B **13**, 5188 (1976).

[36] S.-H. Wei, S. B. Zhang, and A. Zunger, Phys. Rev. B **59**, R2478 (1999).

[37] D. S. Su and S.-H. Wei, Appl. Phys. Lett. **74**, 2483 (1999).

[38] S. R. Hall, J. T. Szymanski, and J. M. Stewart, Can. Mineral. **16**, 131 (1978).

[39] L. O. Brockway, Z. Kristallogr. **89**, 434 (1934).

[40] J. E. Bernard, L. G. Ferreira, S.-H. Wei, and A. Zunger, Phys. Rev. B **38**, 6338 (1988).

[41] R. Magri, S.-H. Wei, and A. Zunger, Phys. Rev. B **42**, 11388 (1990).

[42] A. Janotti and S.-H. Wei, Appl. Phys. Lett. **81**, 3957 (2002).

[43] J. E. Rowe and J. L. Shay, Phys. Rev. B **3**, 451 (1971).

[44] S.-H. Wei and A. Zunger, Phys. Rev. B **49**, 14337 (1994).

[45] S. Chichibu, T. Mizutani, K. Murakami, T. Shioda, T. Kurafuji, H. Nakanishi, S. Niki, P. J. Fons, and A. Yamada, J. Appl. Phys. **83**, 3678 (1998).

[46] J. L. Shay, B. Tell, H. M. Kasper, and L. M. Schiavone, Phys. Rev. B **7**, 4485 (1973).

[47] S.-H. Wei and A. Zunger, Phys. Rev. B **39**, 3279 (1989).

[48] N. Kamoun, H. Bouzouita, and B. Rezig, Thin Solid Films **515**, 5949 (2007).

[49] G. E. Davidyuk, O. V. Parasyuk, S. A. Semenyuk, and Y. E. Romanyuk, Inorg. Mater. **39**, 919 (2003).

[50] A. Bauknecht, U. Blieske, T. Kampschulte, J. Albert, H. Sehnert, M. Ch. Lux-Steiner, A. Klein, and W. Jaegermann, Appl. Phys. Lett. **74**, 1099 (1999).

[51] C. Y. Moon, J. Li, S. H. Wei, Adele Tzu-Lin Lim, and Y. P. Feng, Phys. Rev. B **74**, 205203 (2006).

[52] K. Doverspike, K. Dwight, and A. Wold, Chem. Mater. **2**, 194 (1990).

[53] R. Adhi Wibowo, E. S. Lee, B. Munir, and K. H. Kim, Phys. Status Solidi A **204**, 3373 (2007).

[54] H. Matsushita, T. Ochiai, and A. Katsui, J. Cryst. Growth **275**, e995 (2005).

[55] S. Schorr, H. J. Hoebler, and M. Tovar, Eur. J. Mineral. **19**, 65 (2007).